https://doi.org/10.5194/egusphere-2025-6320
Preprint. Discussion started: 31 December 2025

Response of Rb-Sr system in biotite during contact metamorphism in the aureole of the Makhavinekh Lake Pluton, Labrador

Christopher R.M. McFarlane[1]

[1]Department of Earth Sciences, University of New Brunswick, Fredericton, E3B5M5, Canada

Correspondence to: Christopher R.M. McFarlane (crmm@unb.ca)

Abstract. High-temperature contact metamorphism in the aureole of the 1322 Ma Makhavinekh Lake Pluton, Labrador, led to progressive consumption of 1850 Ma garnet formed during upper-amphibolite facies regional metamorphism that produced migmatitic paragneiss (Tasiyuak Gneiss). Biotite Rb-Sr isotope measurements were carried out in situ by laser ablation MS/MS ICP-MS allowing biotite in a variety of textural settings to be characterized. This natural laboratory provides important constraints on the nature of Rb-Sr closure temperature (*Tc*) as a function of textural setting in high-grade metamorphic rocks. Intact biotite inclusions armoured in garnet preserved in the outer aureole (>4km from the contact) display a range of Rb-Sr isochron ages between ~1850 Ma and ~1322 Ma consistent with a zone of partial retention of Sr in biotite. Isotopic resetting in the outer aureole was controlled by microfractures in garnet that provided short-circuit diffusion pathways for redistribution of radiogenic Sr into plagioclase-bearing contact metamorphic assemblages; biotite inclusions isolated from microfractures retained 1850 Ma Rb-Sr isochron ages. Biotite grains falling along a ~1322 Ma isochron attest to efficient intra- and intercrystalline Sr diffusion at $T \geq 500$ °C on timescales of ≥ 5 Myr. Samples in the central part of the contact aureole (3.7 to 1.1 km from the contact) contain partly resorbed biotite surrounded by contact metamorphic Opx + Crd coronal assemblages in addition to armoured inclusions in relict garnet. These display similar Rb-Sr behaviour to outer aureole samples with the exception that ~1322 Ma biotite domains display higher Rb/Sr due to more extreme loss of Sr. In the inner aureole, where garnet has been completely consumed by contact metamorphic assemblages, a new generation of biotite neoblasts occurs in textural equilibrium with Opx + Crd. This biotite preserves Rb-Sr ages ≤1322 Ma with initial $^{87}Sr/^{86}Sr$ best interpreted as a mixture of radiogenic Sr accumulated in regional biotite and whole-rock Sr liberated from low-Rb/Sr regional metamorphic garnet, apatite, and plagioclase. This study reveals how the exact textural setting of biotite in high-grade metamorphic rocks influences the preservation of Rb-Sr ages and demonstrates that there is no universal closure temperature for biotite Rb-Sr. It also reveals that in situ Rb-Sr dating of granulite or UHT rocks might provide robust chronometric data if grains isolated from intergranular diffusion are systematically evaluated to reveal zones of partial retention.

https://doi.org/10.5194/egusphere-2025-6320
Preprint. Discussion started: 31 December 2025

1 Introduction

The closure temperature (*Tc*) for radiogenic Sr diffusion in biotite has been estimated primarily using empirical studies using conventional mineral separates (Hanson and Gast, 1967; Willigers et al., 2004; Armstrong et al., 1966; Percival and Peterman, 1994). Community consensus on biotite Rb-Sr closure temperatures was strongly influenced by studies such as von Blanckenburg et al (1989), with 300 to 500 °C *Tc* estimates subsequently incorporated into a general knowledge framework (Chiaradia et al., 2013) and later cited in derivative publications (e.g. Nebel, 2015). Most early estimates of biotite Rb-Sr *Tc* attempted to contextualize variations in 'open' vs. 'closed' system isochron ages based on the concepts of Dodson (1973; 1979) and later modifications to volume diffusion expressions (e.g. Ehlers and Powell, 1994; Ganguly and Tirone, 1999). Recognizing the limitations of an 'infinite reservoir' model an attempt was made by Jenkin and co-workers (Jenkin et al., 2001; Jenkin et al., 1995) to review and reconcile Rb-Sr closure in biotite under 'closed-system' conditions and by considering the effect of mineral modal abundance and Sr concentration on isotopic (dis)equilibrium. An important outcome of Jenkin et al (2001; 1995) is that a fixed value for Rb-Sr closure temperature is unlikely in rocks cooling as a closed-system and with variable mineral modes (especially biotite and plagioclase) and grains sizes. However, the influence of the exact microtextural setting of biotite could not be considered using conventional analytical methods. Other studies additionally emphasized the importance of local disequilibrium affected by fluid-rock interactions (e.g. Glodny et al., 2008 and references therein). Recognizing these grain-scale controls on Rb-Sr equilibrium, attempts at micro-sampling and TIMS measurements were also made (Müller et al., 2000; Sousa et al., 2013) that revealed complexities related to the presence of older components in micas and the problem of isotopic disequilibrium in a local reactive matrix.

The advent of MS/MS-ICP-MS technology caused a paradigm shift in how mineral chronometers relying on isobaric β-decay can be utilized. Ground-breaking papers using the laser-ablation (LA) MS/MS-ICPMS in situ Rb-Sr dating method (Hogmalm et al., 2017; Zack and Hogmalm, 2016) have set the stage for a reconciliation of mica closure temperatures. Although the method lacks high absolute precision, Rb/Sr and Sr-isotope variations can now be linked to spatial and textural context, compositional variations, and microstructural features as revealed by careful optical examination or by tools such as electron-backscatter diffraction spectroscopy (EBSD) (Ribeiro et al., 2023).

With the proliferation of in situ Rb-Sr mica studies there is a need to reassess closure temperatures in a variety of natural settings where physico-chemical, textural, and age information is well known. As with some of the earliest contributions to differential closure of mineral chronometers (Harrison and Clarke, 1979; Hanson and Gast, 1967), contact aureoles remain fertile testing ground for closure systematics. Here the well-characterized high-temperature aureole adjacent to the Makhavinekh Lake Pluton (MLP), Labrador, Canada, is used to test for intracrystalline Sr diffusion and the role of intergranular diffusion on biotite Rb-Sr dates. The results demonstrate that dry, diffusion-controlled, metamorphism yield characteristic behaviour in biotite Rb-Sr isotope systematics that represent one end-member of the wide range of processes likely to affect Rb-Sr closure in biotite.

https://doi.org/10.5194/egusphere-2025-6320
Preprint. Discussion started: 31 December 2025

2 Local geology and previous work

The MLP is part of the ca. 1350 to 1290 Ma Nain Plutonic Suite of central Labrador (Fig. 1). It is a 30km wide (1000 km2) composite pluton assembled at ca. 1322 Ma from successive intrusions of cumulate troctolite, anorthosite, and ferrodiorite surrounded by fayalite granite grading outward into hornblende-biotite granite (Ryan, 1991). Zircon extracted from fayalite granite samples produced a concordant TIMS U-Pb zircon age of 1322 ± 2 Ma (McFarlane et al., 2003a). The MLP is in contact with the metasedimentary Tasiuyak Gneiss along its northern and southern margins. The Tasiuyak Gneiss occupies the axial region of the Torngat Orogen and is a relatively lithologically and geochemically homogeneous unit mappable over 400 km of strike length. It is a well-layered metapelitic metatexite paragneiss with alternating layers of Grt + Sil + Bt + Kfs + Qz melanosome and quartzofeldspathic leucosome (abbreviations after Whitney and Evans, 2010). The gneiss experienced peak P-T conditions of ~850° C and 6 to 9 kbar between 1860 to 1850 Ma (Rivers et al., 1996; Van Kranendonk, 1996; Scott and Machado, 1995; Bertrand et al., 1990; Tettelaar and Indares, 2007). These prograde assemblages were overprinted by an orogen-parallel sub-vertical mylonitic fabric with sub-horizontal lineations attributable to left-lateral shearing associated with the Abloviak Shear Zone. Subsequent exhumation and decompression of the Tasiyuak Gneiss in the northern portion of the Torngat Orogen occurred along steeply dipping east-vergent faults with exhumation constrained to the period 1790 and 1750 Ma based on Ar-Ar closure temperatures recorded in hornblende (Mengel and Rivers, 1997; Mengel et al., 1991). This period of near-isothermal decompression produced thin fine-grained symplectitic coronas of Opx ± Pl on garnet and rare fine-grained Spl + Crd symplectite replacing sillimanite.

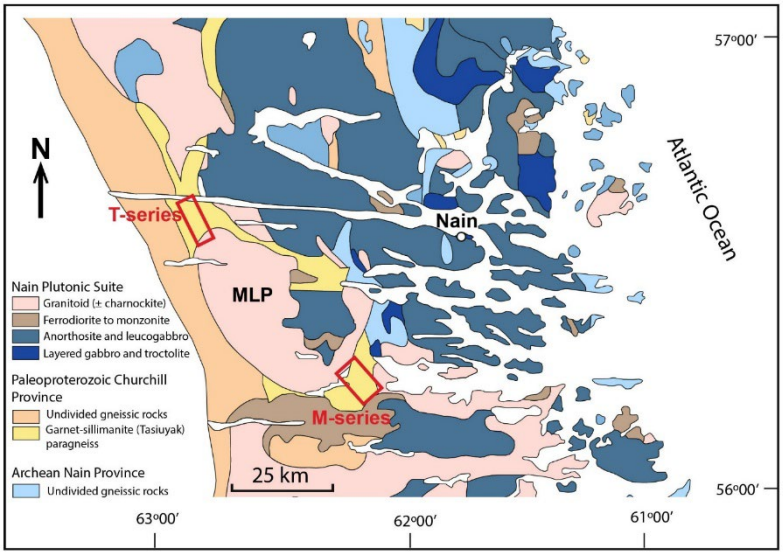

Figure 1. Location of the Makhavinekh Lake Pluton (MLP), host Tasiyuak paragneiss, and the surrounding Nain Plutonic Suite intrusions in the vicinity of Nain, coastal Labrador. Samples for this study were selected from two previously described transects from the northern (T-series samples) and southeast (M-series samples) contact zones of the MLP. Modified from Lightfoot et al (2012).

https://doi.org/10.5194/egusphere-2025-6320
Preprint. Discussion started: 31 December 2025

Contact metamorphism of the Tasiyuak Gneiss during intrusion of the MLP had a profound impact on the inherited regional textures and mineralogy. Several studies (McFarlane et al., 2003a; Tettelaar and Indares, 2007; Kelly et al., 2011; Mariga et al., 2006) have shown that ~1850 Ma garnet is progressively replaced by diffusion-controlled coronas comprising Opx + Pl and Opx + Crd ± Pl. The overall character of the contact metamorphic coronal assemblages and surrounding quartz-plagioclase-K-feldspar leucosome is well-illustrated using in micro-X-ray fluorescence (µXRF) mapping (Fig. 2; sample M04-450m). This shows the localization of calcic plagioclase as part of the outermost coronal assemblage that is followed inward by symplectitic Opx + Crd. Plagioclase also locally occurs intergrown with blocky orthopyroxene that preferentially formed adjacent to quartz inclusions in garnet and quartz in the matrix bordering garnet. Thickness and grain size of coronal assemblages increases with decreasing distance to the MLP contact; the last remnants of garnet are consumed at distances <500 m.

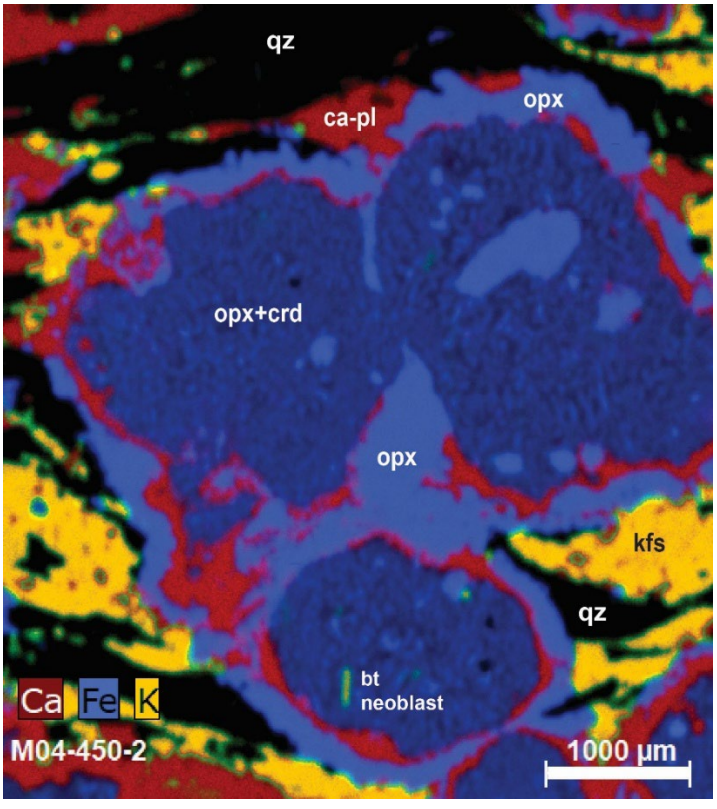

Figure 2. Micro-XRF elemental map for contact-metamorphic assemblages replacing regional metamorphic garnet in the Tasiyuak paragneiss. Sample at 450m from contact. Tectonized leucosomes comprise deformed quartz, K-feldspar, and plagioclase. These anastomose around regional metamorphic garnet that is replaced by contact metamorphic coronal assemblages of Opx + Ca-Pl and Opx + Crd ± Bt. A biotite neoblast is present in the lowermost corona.

Although the exact garnet breakdown reaction varies as a function of local bulk composition and inclusion suites, Mariga et al (2006) envisioned a net-transfer reaction of the form: Grt + Bt + Qz = Crd + Opx + Kfs + OH. Note, however,

https://doi.org/10.5194/egusphere-2025-6320
Preprint. Discussion started: 31 December 2025

that a new generation of biotite locally forms in textural equilibrium with Opx + Crd symplectite and this model reaction could be modified to include this biotite as an additional product acting as a sink for K, Rb, and OH. Breakdown of garnet is also accompanied by consumption of sillimanite to coarse coronal assemblages dominated by hercynitic-Spl + Crd. A less obvious transformation sees rutile replaced by ilmenite in the inner aureole. The composition of biotite across the MLP aureole shows only minor variability as a function of textural setting. Work by Tettelar and Indares (2007) documented regional metamorphic biotite with *X*Fe 0.24-0.26, 4.5 to 5.7 wt% TiO_2 and predominance of F > Cl in the OH site. Contact metamorphic biotite within coronal assemblages after garnet in the inner aureole is slightly more magnesian (*X*Fe 0.22-0.24) but with similar TiO_2 and F content owing to the similarity between peak regional temperatures and those encountered in the inner aureole. The timing of these coronal assemblages is unequivocally dated at 1322 Ma based on SHRIMP dating of neoformed Y-rich monazite that nucleated as coronal overgrowths on large pre-existing 1850 Ma grains (McFarlane et al., 2005b). Contact metamorphic temperatures in the Tasiuyak Gneiss immediately adjacent to the intrusive contact (<100 m) reached >800°C as recorded by high Al concentrations in symplectitic orthopyroxene, pervasive dynamic recrystallization and polygonization of contact assemblages, and local production of anatectic melt films surrounding resorbed quartz, K-feldspar, and plagioclase. In contrast Grt-Opx, Grt-Crd, and Crd-Spl FeMg-exchange thermometry records temperatures of ~575°C at all distances in the aureole. This is interpreted as a retrograde cooling temperature and is taken as a minimum temperature achieved in the aureole.

The *T-t* paths, as a function of distance from the intrusive contact (assuming P = 4 kbar), have been previously estimated using both conductive one-dimensional analytical and multi-stage two-dimensional finite-difference models (McFarlane et al., 2003b). More robust numerical modelling with convective cooling implemented in HEAT3D (Wohletz et al., 1999) suggest peak-*T* of 554 °C would be reached at 6 km distance after 3.5 Myr with cooling below 500 °C after ~15 Myr. Rocks in the central aureole at 3 km distance are modelled to reached peak-*T* of 680 °C after 5 Myr and then cool below 500 °C after >20 Myr. Rocks in the inner aureole would have rapidly reach peak-T >800 °C and cooled below 500 °C after ~30 Myr. Thus, biotite that remained 'open' to Sr diffusion above 500 °C is expected to record isochron ages <1310 Ma in the outer aureole and <1295 Ma in the inner aureole.

The MLP aureole has been used to test isotopic robustness in a variety of minerals and decay systems. Zircon separated from Tasiyuak Gneiss from various distances from the contact was used to document, using SHRIMP analyses, intracrystalline redistribution of Pb during recovery of metamict domains (McFarlane et al., 2005a). Large monazite grains separated from the same samples were used to assess Pb-diffusion using a SIMS depth-profiling technique (McFarlane and Harrison, 2006). A combination of garnet trace-element zoning and conventional Lu-Hf geochronology was used by Kelley et al. (2011) to document the effect of garnet resorption on preservation of garnet-ilmenite Lu-Hf isochron ages. In all of these studies the progressive effects of contact metamorphism are shown to be systematic in terms of mineralogical, mineral-chemical, and isotopic changes.

https://doi.org/10.5194/egusphere-2025-6320
Preprint. Discussion started: 31 December 2025

3 Sample selection and description

Samples of the Tasiyuak Gneiss were examined along two transects previously documented by McFarlane et al. (2003) and Kelley et al (2011): one approaching the northern contact of the MLP (T-series samples) the other along its southeastern margin (M-series samples). Triage of the samples showed that the M-series preserves fresher assemblages containing biotite suitable for this study. Two samples <5 m from the contact were also included from the T-series suite. The samples were chosen to include a common regional metamorphic assemblage containing Grt-Sil-Bt-Kfs-Pl-Qz with accessory rutile/ilmenite, monazite, zircon, apatite and rare pyrrhotite.

The selected samples are divided into four groups based on distance from the intrusion (given in meters from contact), textures, and contact metamorphic mineral assemblages: 1) M12-4025m, T02-4560m and T03-5750m in the outer aureole with preserved regional assemblages containing biotite armoured in garnet and pristine rutile; 2) M10-3700m, M09-2380m, and M20A-1100m at intermediate distances with partly-consumed garnet and biotite liberated to the coronal assemblages and well-preserved rutile; 3) T28-2m, M02C-10m and T08-15m from the inner aureole with biotite neoblasts in textural equilibrium with the contact metamorphic assemblages; 4) T28-2m additionally contains biotite that forms an intergranular melt-pseudomorph film between ovoid quartz and feldspars.

Plane light photomicrographs of the four main textural groups are illustrated in Fig. 3. Samples from the outer aureole contain large garnet porphyroblasts with clustered inclusions of fine sillimanite needles that locally preserved a relict S-C fabric. Garnet hosts sub-rounded inclusions of brown biotite, locally aligned with internal fabrics, ovoid to elongate quartz inclusion, rounded ilmenite, minor apatite, and rare plagioclase. Abundant microfractures in garnet are oriented at a high angle to the proto-mylonitic layering. Garnet is wrapped by layers composed of perthitic K-feldspar, minor plagioclase, ribbon quartz, coarse-grained sillimanite and dark honey-brown rutile, and patches of foliated brown biotite. Biotite also forms irregular decussate overgrowths surrounding ilmenite and within pressure shadows surrounding garnet; this biotite is assumed to be retrograde after M2 contact metamorphism and was avoided. Garnet and sillimanite in close contact (e.g. <500 um) display growth of fine-grained coronal assemblages.

https://doi.org/10.5194/egusphere-2025-6320
Preprint. Discussion started: 31 December 2025

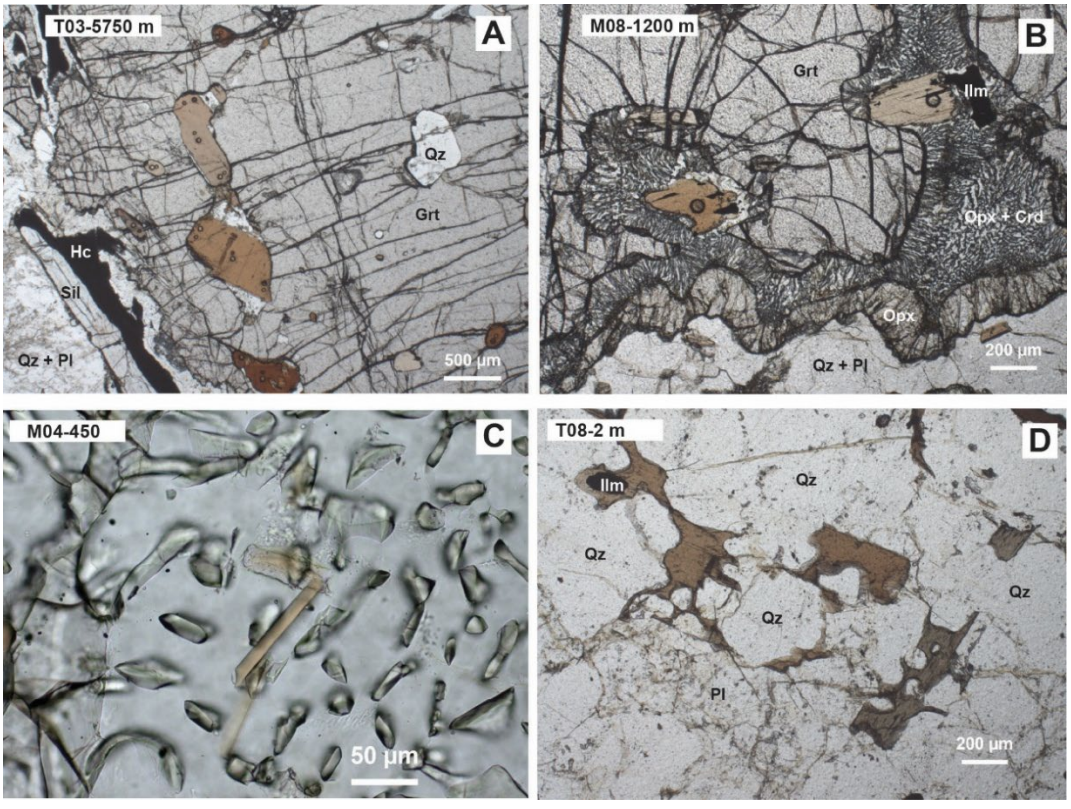

Figure 3. Plane light photomicrographs of key mineralogical and textural relationships in the MLP contact aureole. A) Sample T03 from the outer aureole contains large oblate biotite and quartz inclusions in heavily microfractured garnet. Several 48 µm diameter laser craters are visible in brown biotite. B) In the central part of the aureole large biotite grains can locally be found surrounded by symplectitic Opx + Crd. These grains display cuspate grain boundaries that suggest evidence of reaction. Laser craters (48 µm) also visible. C) Coronal assemblages in the inner aureole locally contain subidioblastic biotite neoblasts in textural equilibrium with Opx + Crd. D) Immediately adjacent to the MLP contact the Tasiyuak Gneiss displays irregular optically-continuous lobate patches of brown biotite that form interstitial domains with low dihedral angles between sub-rounded quartz and plagioclase grains

Samples centrally located in the aureole record the growth of thicker layered coronae around garnet and sillimanite. A monomineralic orthopyroxene corona, 50-100µm thick, marks the boundary between garnet rim and neighbouring quartzofeldspathic matrix. Similar monomineralic orthopyroxene coronae form internally along the interface between ovoid quartz inclusions and host garnet. Symplectitic Opx + Crd ± Pl coronae occur between the remaining garnet and the outermost Opx corona. Slender prisms of orthopyroxene and intervening cordierite form perpendicular to the reacting garnet interface. Symplectitic assemblages are also preferentially developed along pre-existing microfractures. These corona assemblages ultimately intercept biotite that was previously armoured in garnet. In these settings the portion of biotite in contact with the symplectitic minerals takes on a ragged appearance that contrasts with the smooth curvilinear boundaries of armoured biotite inclusions. This suggests biotite breakdown as armoured grains joined the M2 assemblage. The Spl + Crd symplectitic coronae around sillimanite at intermediate distances also display a layered structure, with an outer

https://doi.org/10.5194/egusphere-2025-6320
Preprint. Discussion started: 31 December 2025

monomineralic cordierite corona surrounding a symplectitic mixture of Spl + Crd. Rutile is locally replaced by ilmenite in intermediate samples where rutile is proximal to garnet. Rutile armoured in quartz of feldspars in leucosomes remain pristine and easily identified optically.

Samples in the inner aureole (<100 m) have no relict garnet or sillimanite preserved. Here the coronal assemblages are coarse and more randomly oriented suggesting they experienced textural reconfiguration by secondary grain growth. No relict biotite is present. Rather, platy biotite neoblasts (20-100 μm wide, up to 500 μm long) occur in textural equilibrium with Opx + Crd ± Kfs. Biotite is rare in the layered matrix of these rocks, but it occurs in patches, locally as partially vermicular pods adjacent to coronas, that could be diagnostic of in situ melt crystallization. The quartzofeldspathic layers in the most proximal inner aureole rocks also display evidence for partial melting such as rounded quartz surrounded by irregular grain-boundary films of biotite and K-feldspar that form with shallow dihedral angles against adjacent quartz grains. These are best interpreted as sites of in situ melt crystallization (so-called 'melt pseudomorphs') and implies small degrees of partial melting under low aH_2O conditions at $T > 800°C$ at < 4.

4 Methods

This work was carried out using a combination of optical microscopy, LA ICP-MS for trace-element quantification and in situ Rb-Sr measurement using laser ablation MS/MS ICP-MS. Optical microscopy in transmitted and reflected light was used to characterize the textural setting and morphology of biotite grains as a function of proximity to the MLP intrusive contact.

The Rb-Sr isotope ratios in biotite were measured by LA MS/MS-ICP-MS using an Applied Spectra Inc. RESOlution™ 193nm laser system equipped with a Laurin Technic Pty. S-155 large format ablation cell that is connected to an Agilent 8900 'QQQ' ICP-MS. Laser crater diameters ranged from 66 to 33 μm depending on the size of biotite targets. Laser fluence of 2 J/cm^2, pulse rate of 7 Hz, and ablation time of 40 sec were used as standard operating settings. A mixed carrier gas of pure He (300 mL/min), Ar (900 mL/min), and N_2 (1.8 mL/min) were used to transfer ablated aerosols to the mass spectrometer via two in-line Laurin Technic Pty 'squid' smoothing devices. For Rb-Sr isotope measurement the Agilent 8900 was operated in in mass-shift mode using 10% SF6 (balance He) as the reaction gas. The analyte list included ^{39}K, ^{44}Ca, ^{85}Rb, ^{104}RbF, ^{86}Sr, ^{105}SrF, ^{87}Sr, ^{106}SrF, ^{88}Sr, and ^{107}SrF. The instrument was tuned while rastering on NIST610 to maximize counts on mass-shifted Sr while maintaining low RSD signals. This occurred at SF6 flow rate of 28-30% and with a small amount of H_2 added (1-2% flow). Calibration of pulse/analog (P/A) factors was also carried out before each analytical session using NIST610 and an in-house apatite from Phalabowra, South Africa, with ~4000 ppm Sr; this ensures that variations in ion beam intensity for mass-shifted ^{105}SrF, ^{106}SrF, and ^{107}SrF among standards and samples was fully linearized between detector modes. The signal for ^{85}Rb cps is typically counted in analog mode (> ~1.4 Mcps). Net counts at mass ^{105}RbF was 0 attesting to the efficient online separation of Rb from Sr.

https://doi.org/10.5194/egusphere-2025-6320
Preprint. Discussion started: 31 December 2025

The S-155 cell accommodates 6 polished thin sections and 5 epoxy 1" round standard blocks. In all analytical sessions the standards included MicaMg-NP (myStandards GmbH, with reference isotope values from Hogmalm et al 2017), NIST610 glass, and an in-house biotite standard from the Loch Borralan syenite complex, Scotland (~430 Ma). Each analytical session comprised 15 measurements of each certified and in-house standard that were interspersed with the unknowns. The data was reduced offline using a custom DRS in Iolite4™. A mass bias in Rb/Sr arises during LA MS/MS-ICP-MS between MicaMg-NP and natural crystalline biotite; this typically manifests as a systematic offset in $^{87}Rb/^{86}Sr$ on the order of 3-5% across all analytical sessions; no systematic bias in $^{87}Sr/^{86}Sr$ or $^{88}Sr/^{86}Sr$ was observed. Thus, an empirical correction is calculated and applied to $^{87}Rb/^{86}Sr$ to bring in-house secondary standards in-line with known crystallization ages. This correction is then applied to the unknowns assuming similar mass bias behaviour. No additional error was added to unknowns during the normalization step. Initial Sr in regional metamorphic rocks was measured on plagioclase in leucosomes in sample T03-5750m using the same methodology but with NIST610 used as a standard for $^{87}Sr/^{86}Sr$. The weighted mean measured value of 0.730 ± 0.001 is used to anchor isochrons when necessary. Plotting isochrons and linearized probability plots and derivative age calculations were performed using Isoplot4.3 (Ludwig, 2012) and using a ^{87}Rb decay constant of 1.3972E-11 a^{-1}. Model-1 regressions, taking into account measured errors and error correlations in the dataset, are reported unless noted otherwise. Errors on model age calculations were assigned based on the 2SE measured on the $^{87}Rb/^{86}Sr$ (typically 2-5%). Data tables for Rb-Sr can be found in the supplement.

5 Results

5.1 Armoured biotite in outer aureole

A total of 88 Rb-Sr measurements were obtained on armoured grains in outer aureole samples. The full Rb-Sr isotopic dataset is shown on a normal isochron diagram in Fig. 4. Reference isochrons for 1850 Ma and 1322 Ma are also shown. Each of the three samples analysed at this distance contain spots on armoured grains that preserve a Rb-Sr isochron age that overlaps with the timing of ~1850 Ma regional metamorphism. By filtering this dataset for spots with model ages > 1800 Ma it is possible to calculate an anchored regression yielding 1846 ± 19 Ma (n =11). The linearized probability plot for model ages of individual spots calculated for this dataset produces a characteristic S-shaped distribution with a slope that is far-removed from the value of 1.0 predicted for a single (normally distributed) population containing only systematic (internal) error. An anchored regression of the four points with youngest model ages in this dataset produce an age of 1313 ± 43 Ma with MSWD = 16.

https://doi.org/10.5194/egusphere-2025-6320
Preprint. Discussion started: 31 December 2025

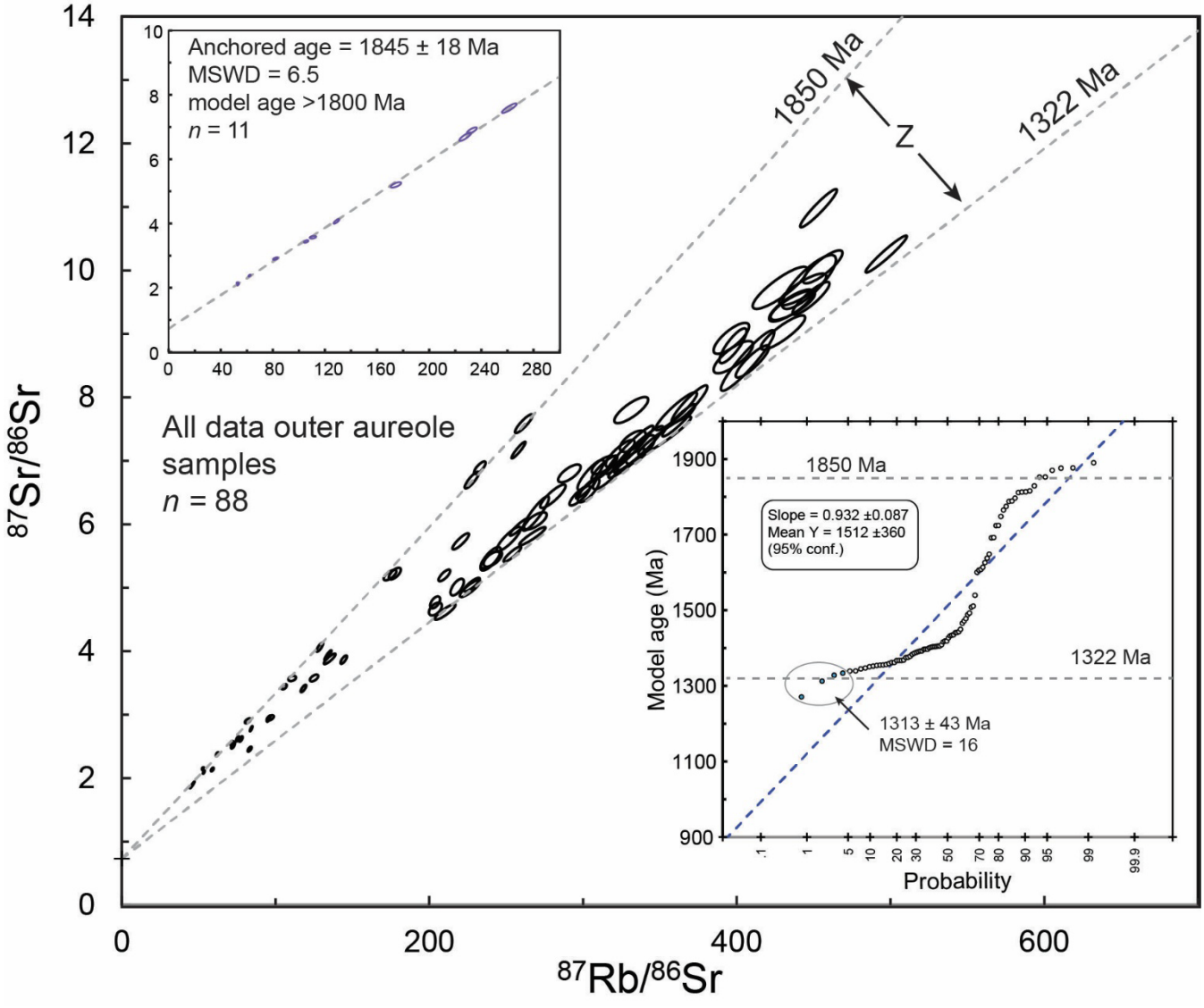

Figure 4. Rb-Sr results for biotite inclusions in garnet for outer aureole samples. Reference isochrons for 1850 Ma and 1322 Ma were calculated at initial $^{87}Sr/^{86}Sr$ =0.73. The distribution of data points defines a zone of partial retention 'Z' between these two reference lines. A gradual shift in $^{87}Rb/^{86}Sr$ to higher values accompanies resetting of 1850 Ma biotite. Inset diagram: linearized probability plot (error bars excluded for clarity) showing 'S'-shaped distribution characteristic of a zone of partial retention with calculated anchored 4-point isochron for youngest analyses in this dataset.

5.2 Biotite liberated to coronas in central aureole

A total of 115 Rb-Sr measurements were obtained on biotite grains in three distinct textural settings in samples M10-3700m, M09-2380m, and M20A-1100m: 1) fully armoured in garnet; 2) partly liberated; 3) fully surrounded by the symplectitic coronal assemblage. The full dataset is shown in Fig. 5. The distribution of Rb-Sr data in these three samples is similar to

https://doi.org/10.5194/egusphere-2025-6320
Preprint. Discussion started: 31 December 2025

the outer aureole dataset except for two grains, from partly and fully liberated biotite grains, that have Rb/Sr >1000. Only completely armoured biotite grains preserve regional metamorphic ages. Filtering analyses of armoured biotite grains to extract those with model ages >1800 Ma (n = 17) produces an anchored isochron age of 1852 ± 18 Ma. Biotite grains that are partly liberated from garnet (n =29, 1 rej.) define a raw regression of 1381 ± 46 Ma with initial $^{87}Sr/^{86}Sr$ = 0.772 ± 0.089 and MSWD = 57. The high MSWD values reflects a spread of data within the zone of partial retention. Biotite in full contact with coronal assemblages (n = 50, 1 rej.) produces a Rb-Sr age of 1320 ± 20 Ma with initial of 0.819 ± 0.044 and MSWD = 15. Although this regression displays less scatter, model ages still range from 1284 to 1427 Ma. A linearized probability plot for model ages reveals the four-youngest analyses (all on fully liberated grains) that yield an anchored regression 1292.1 ± 6.5 Ma with MSWD = 0.90.

https://doi.org/10.5194/egusphere-2025-6320
Preprint. Discussion started: 31 December 2025

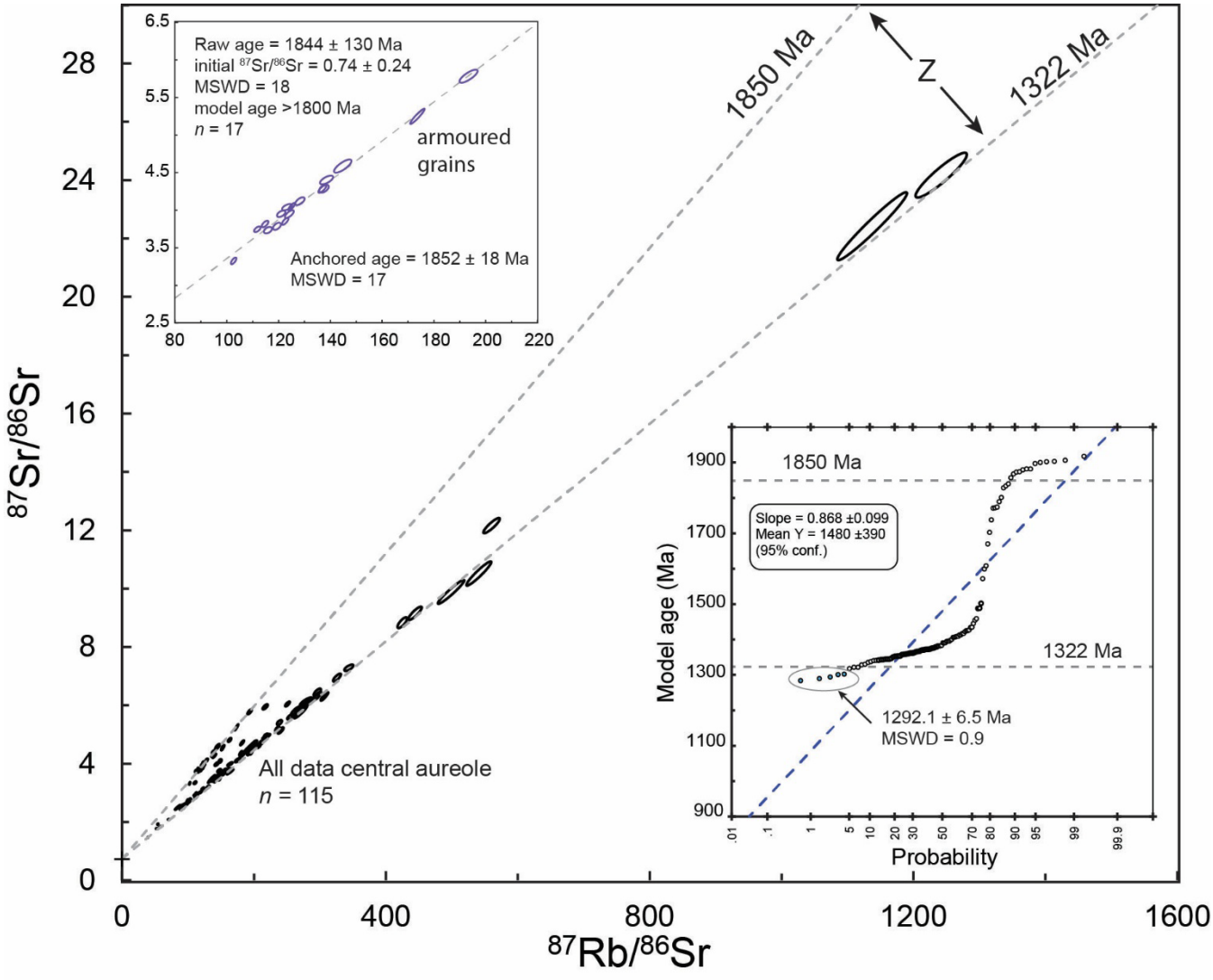

Figure 5. Rb-Sr results for central aureole. Overall, the data display a zone of partial retention similar to the outer aureole. In detail, regional metamorphic ages (inset top left) are recorded only by biotite grains that remained armoured in garnet. The inset linearized probability plot (error bars excluded for clarity) is similar to the outer aureole dataset and the four youngest model ages generate a low-MSWD anchored regression.

5.3 Biotite neoblasts in inner aureole

A total of 60 Rb-Sr measurements were obtained on biotite neoblasts in textural equilibrium with symplectitic assemblages in samples T08-15m, M02A-12m, and T28-2m (Fig. 6). The $^{87}Rb/^{86}Sr$ in these samples spans a range from <50 to >3000 and the raw regression (n = 57, 3 rej.) produces an isochron of 1320.5 ± 7.0 Ma, initial $^{87}Sr/^{86}Sr$ =0.723 ± 0.042, and MSWD = 7.3. Considering model ages anchored at initial $^{87}Sr/^{86}Sr$ = 0.73 half of the points (n =28) have model ages <1322 Ma in the range 1269 Ma to 1322 Ma. The other half of the data has model ages ranging from 1322 to 1357 Ma. This disparity is

https://doi.org/10.5194/egusphere-2025-6320
Preprint. Discussion started: 31 December 2025

evident on a model age linearized probability plot where instead of an S-shaped profile characteristic of a zone of partial retention, the data define a gentled curved array. The portion of the data with model age <1322 Ma yields a statistically robust isochron age of 1303.1 ± 7.0 Ma and initial Sr of 0.721 that overlaps the whole-rock value. In contrast, data with model age >1322 Ma produces a similarly robust isochron age of 1338.4 Ma ± 6.5 Ma and initial Sr of 0.729. Whereas each of these regressions is statistically robust the age of biotite neoblasts must be <1322 Ma. The cause of the discrepancy between 'true' versus measured Rb-Sr ages is addressed below in the discussion.

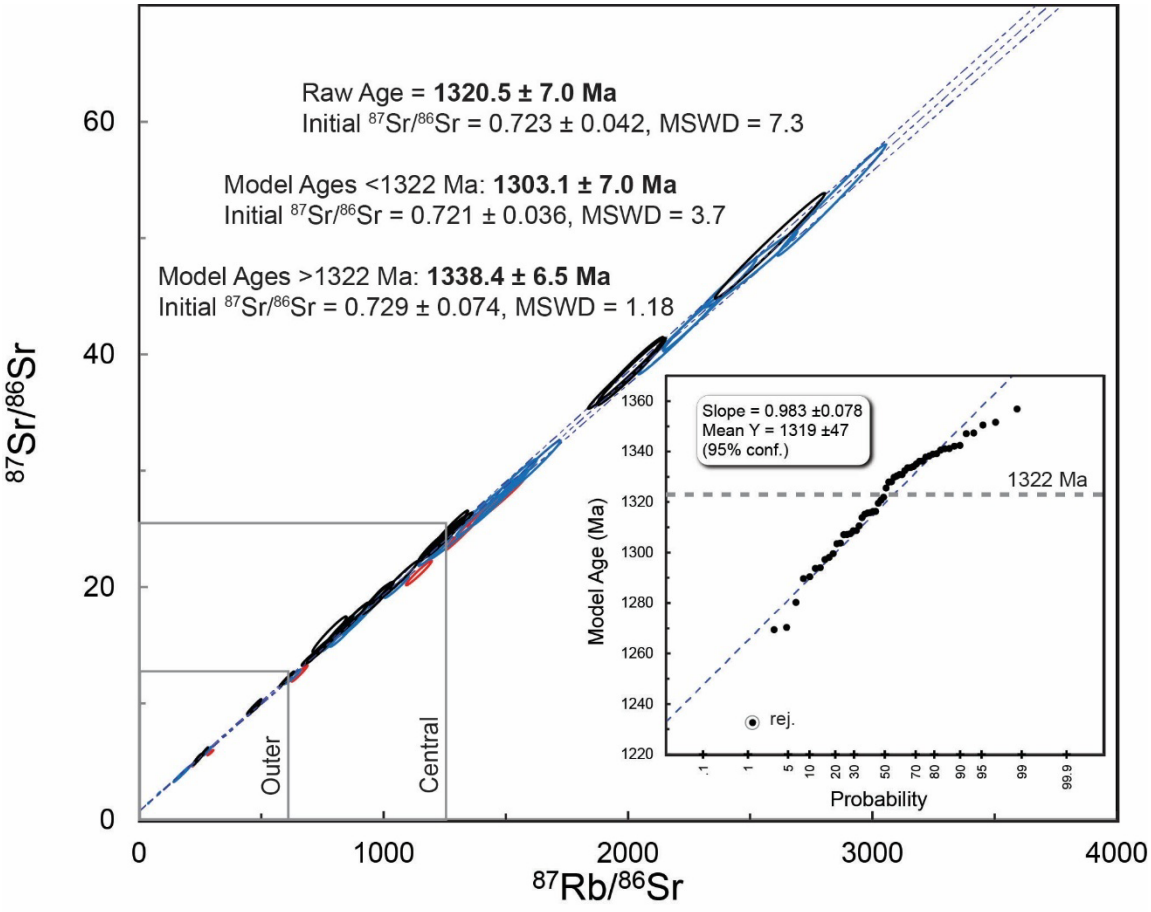

Figure 6. Rb-Sr data for neoblastic biotite grains in textural equilibrium with Opx + Crd corona in the inner aureole. Boxes show range of isotope ratios encountered in the outer and central aureoles. The raw regression overlaps the known crystallization age of the MLP as well as the initial Sr recorded in plagioclase. Regression age and intercepts for data with model ages above or below 1322 Ma (anchored at I_{Sr} = 0.73) are also shown. Inset linearized probably plot for model ages (error bars excluded for clarity) reveals a gently curving array. One anomalously young point was rejected for calculation purposes.

This generation of biotite also displays significant inter- and intracrystalline variability in $^{87}Rb/^{86}Sr$. Exploratory $^{87}Rb/^{86}Sr$ laser mapping of large biotite inclusions in the outer aureole failed to reveal measurable heterogeneity. In contrast, biotite neoblasts large enough to accommodate multiple 26 µm diameter craters display $^{87}Rb/^{86}Sr$ that can vary by almost a factor of two from one end of the grain to the other. An example of a series of biotite neoblasts analysed in sample M02C-

https://doi.org/10.5194/egusphere-2025-6320
Preprint. Discussion started: 31 December 2025

10m is shown in Fig. 7. The wide intracrystalline spread in $^{87}Rb/^{86}Sr$ allows calculation of single-grain ages in cases where three or more individual measurements were performed. Five grains in samples M02C-10 and one grain in T28-2m satisfied these criteria and yielded the following ages when anchored at initial $^{87}Sr/^{86}Sr = 0.73 \pm 0.01$: 1322.5 ± 9.1 Ma, 1312 ± 10 Ma, 1303 ± 50 Ma, 1324.6 ± 8.2 Ma, 1324 ± 42 Ma and 1330 ± 21 Ma. The weighted mean of this population of six grains is 1321 ± 5 Ma.

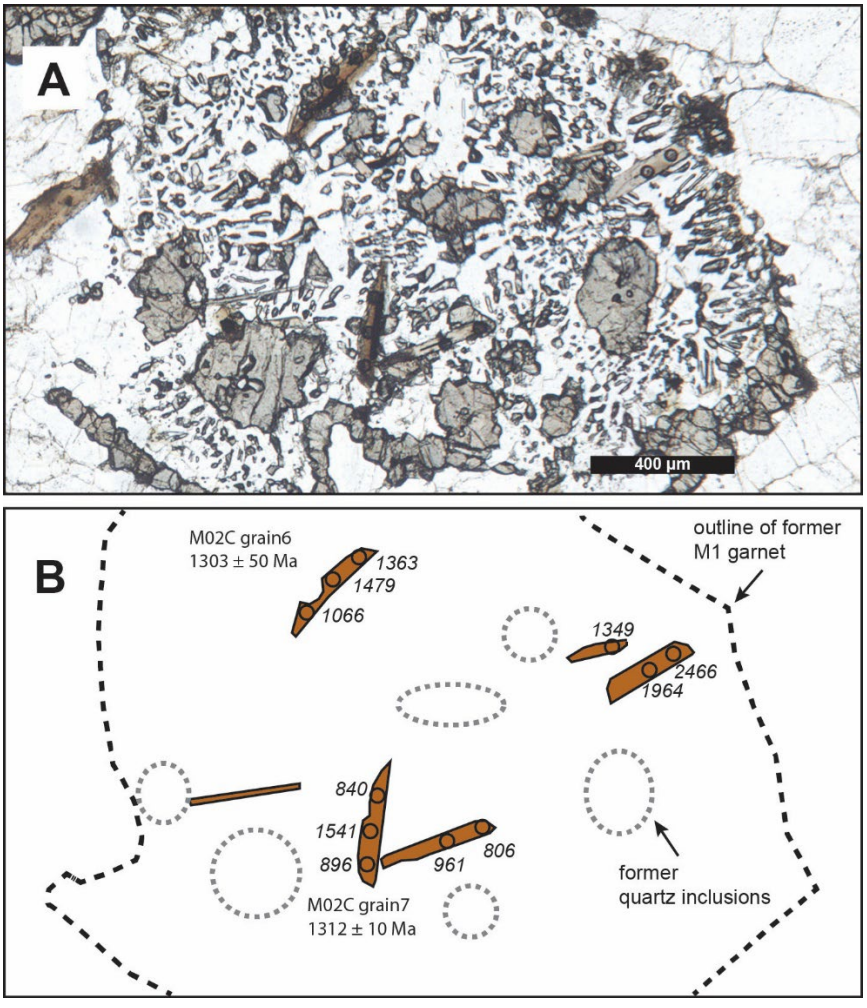

Figure 7. Detail of biotite neoblasts in inner aureole sample M02C-10. A) Plane light photomicrograph showing the locations of 26µm diameter laser craters distributed across individual grains. B) Line drawing illustrating biotite neoblasts and associated $^{87}Rb/^{86}Sr$ at the laser sample locations shown by black circles. Anchored three-point isochron ages are shown for two grains.

5.4 Biotite as interstitial melt-pseudomorphs

Sample T28-2m, immediately adjacent to the intrusive contact contains biotite and micro-perthitic K-feldspar that form as cuspate interstitial domains with low dihedral angles between sub-rounded quartz grains, a texture reminiscent of anatectic

https://doi.org/10.5194/egusphere-2025-6320
Preprint. Discussion started: 31 December 2025

melt pseudomorph patches (e.g. Holness and Clemens, 1999). A total of 22 measurements were obtained on these domains (Fig. 8). The data fall within a narrow range of $^{87}Rb/^{86}Sr$ from ~400 to ~800 which increases uncertainty on the regression compared to the more widely dispersed Rb/Sr values in the other samples. Two data points with anomalously low $^{87}Sr/^{86}Sr$ and elevated Ca concentration may have hit apatite inclusions and were rejected to avoid a negative initial $^{87}Sr/^{86}Sr$ intercept. This results in an isochron date of 1335 ± 66 Ma and a poorly defined initial Sr of 0.71 ± 0.60 with MSWD = 8.6. Anchoring this dataset at 0.730 ± 0.001 brings the age down to 1332.2 ± 8.4 Ma which is just outside error the presumed crystallization age of the MLP. An initial $^{87}Sr/^{86}Sr$ of >0.82 is required to obtain <1322 Ma age for these contact metamorphic melt products.

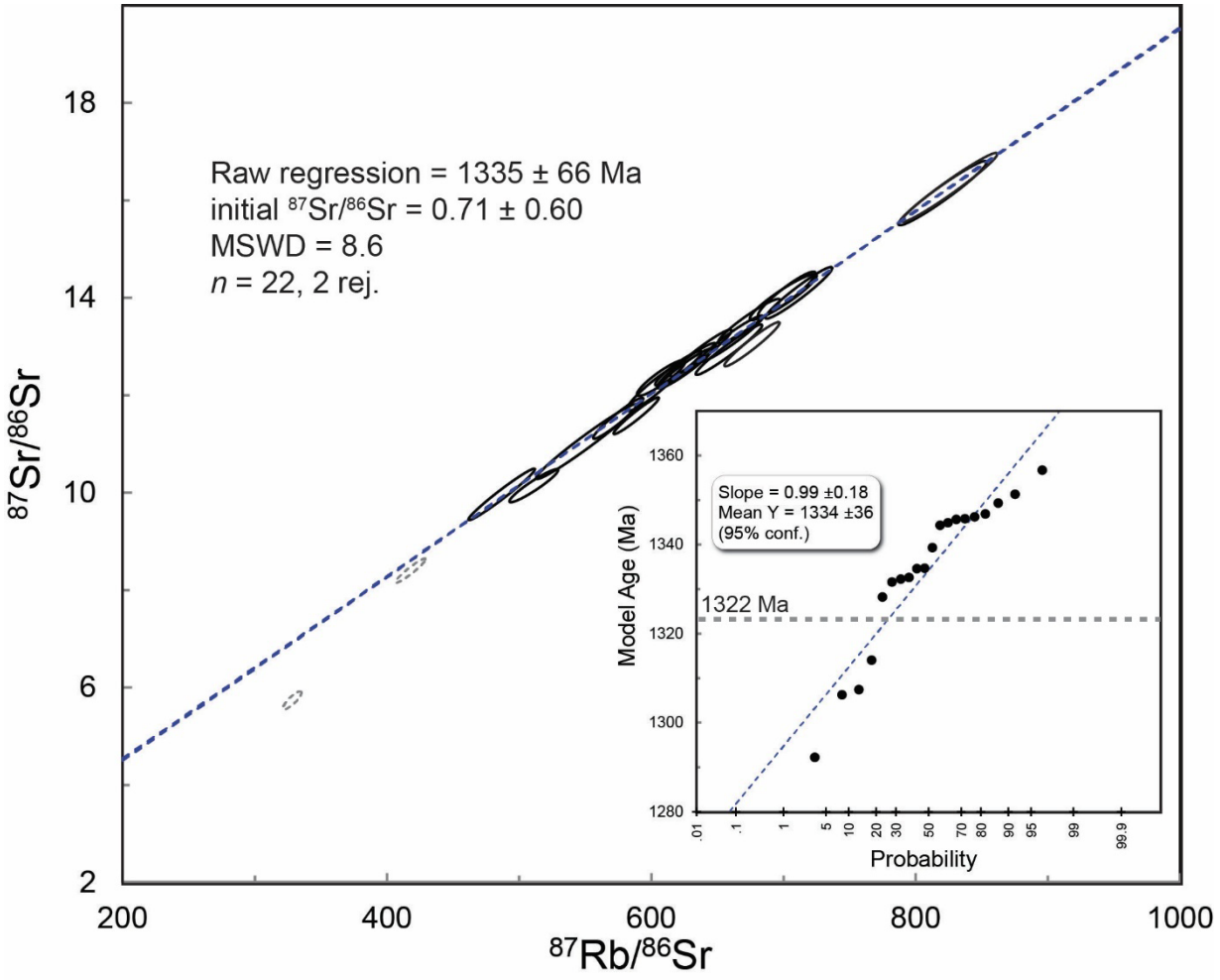

Figure 8. Rb-Sr data for biotite that occurs as melt-film pseudomorphs in Tasiyuak Gneiss at the contact with the MLP. This textural variety of biotite is characterized by a narrow range of $^{87}Rb/^{86}Sr$. Dotted ellipses were rejected from the regression calculation (see text for details). The inset linearized probability curve was generated with model ages calculated at initial $^{87}Sr/^{86}Sr$ = 0.73.

https://doi.org/10.5194/egusphere-2025-6320
Preprint. Discussion started: 31 December 2025

6 Discussion

6.1 Veracity of calculated isochron ages

The discussion of Rb-Sr behaviour in the MLP contact aureole is predicated on the accuracy of in situ Rb-Sr regressions obtained through primary standardization with MicaMg-NP and a secondary standard, phlogopite from the 430 Ma Loch Borralan melanite syenite, Scotland, to correct for mass bias on $^{87}Rb/^{86}Sr$. The contact aureole of the MLP provides an opportunity to test the internal consistency of this standardization approach since the timing of biotite growth must have occurred at either ~1850 Ma or ≤1322 Ma. Five analytical sessions using Loch Borralan phlogopite produced a pooled regression (standardized to MicaMg-NP) of 452 ± 7 Ma with a raw initial $^{87}Sr/^{86}Sr$ =0.706 ± 0.002 (MSWD = 1.9; 2SE). This initial-Sr intercept overlaps within error previous whole rock measurements for the Loch Borralan syenite and all corrected isochrons for this phlogopite are anchored at a value of 0.7055 ± 0.0005 (Thirlwall and Burnard, 1990). Some of the error in this raw age is a result of different crater sizes, and hence different laser-induced Rb/Sr fractionation, required to analyse biotite in different textural settings in the MLP aureole. Orientation effects (Larson et al., 2025) were mitigated as much as possible in both standards and unknowns but it is impossible to eliminate all this potential bias. Inter-session correction factors between 1.025 and 1.075 were required to correct raw $^{87}Rb/^{86}Sr$ to obtain the true age of 430 Ma for Loch Borralan. Reproducibility of the data reduction and correction scheme is supported by the subset of armoured biotite in the outer and central aureole that yield an isochron age of 1853 ± 38 Ma and initial $^{87}Sr/^{86}Sr$ =0.728±0.063 (MSWD = 15). These values overlap with: 1) conventional and in situ U-Pb 1850 Ma dates for zircon and monazite in migmatitic Tasiyuak Gneiss, and; 2) a mean initial $^{87}Sr/^{86}Sr$ of 0.7301±0.0010 (1 of 23 rej. MSWD = 1.2) independently measured on plagioclase in leucosomes. Thus, both the age and initials of corrected regressions overlap known constraints for these rocks.

6.2 Closed- vs. open-system behaviour of Sr

The zone of partial retention recorded in the outer- and central aureole samples is unequivocal evidence for intracrystalline Sr diffusion in biotite. Even some of the largest biotite inclusions in garnet (~200 µm diameter) have been reset to ~1322 Ma Rb-Sr ages. A petrographic examination of garnet and its armoured biotite inclusions suggests that Rb/Sr re-equilibration during contact metamorphism in the outer aureole was most likely controlled by microfractures that produced 'short-circuit' diffusion pathways for Sr. Most texturally intact biotite inclusions in garnet show a systematic decrease in Sr concentration, a shift to higher Rb/Sr, and a decrease in model age towards a 1322 Ma reference line (Fig. 9). This process occurred at peak contact metamorphic temperature and timescales in the outer aureole of ~550°C and a few Myr and implies efficient intra- and intercrystalline diffusion of Sr under these conditions. There is no correlation between model age and Rb concentration observed in the outer aureole; this is consistent with the compatible nature of Rb^+ in the biotite lattice. In addition to plagioclase in the tectonized leucosomes surrounding garnet, incipient breakdown of regional 1850 Ma garnet also produced coronas that locally include calcic-plagioclase as the main host for the grossular component liberated from garnet. Acting as a host for Sr in coronas, this plagioclase provides a convenient sink for the redistribution of Sr from biotite

https://doi.org/10.5194/egusphere-2025-6320
Preprint. Discussion started: 31 December 2025

along microfractures in the host garnet crystal; a similar source-and-sink model was advocated by Jenkin et al. (2001) in their model for Rb-Sr cation-exchange re-equilibration during cooling from lower amphibolite-facies conditions.

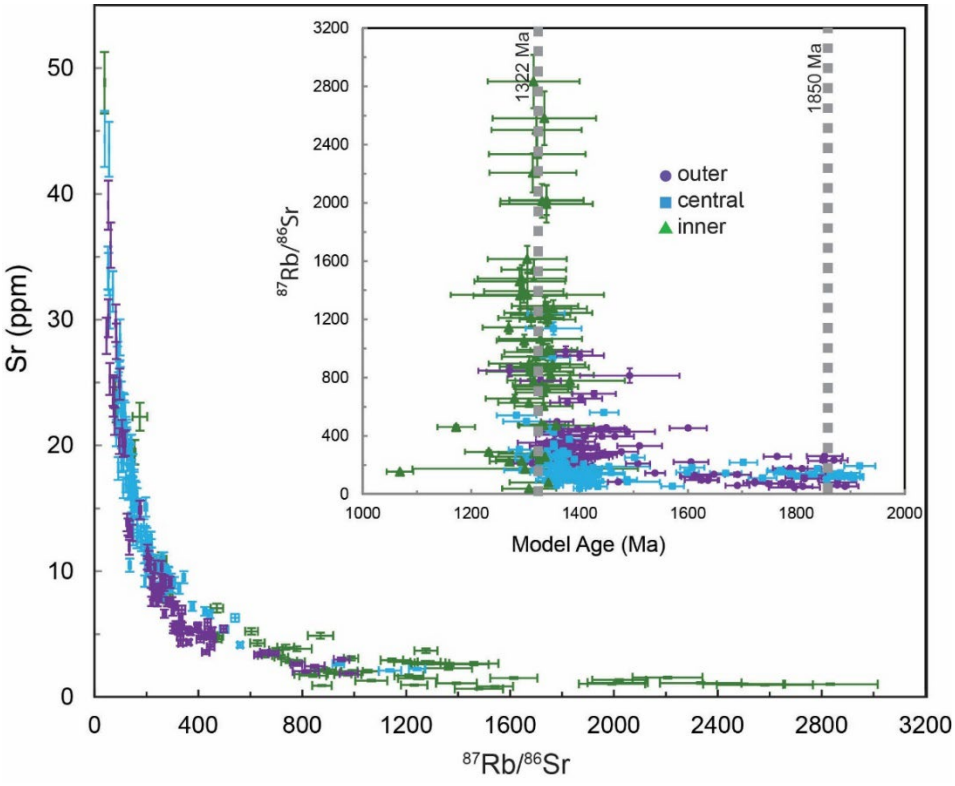

Figure 9. Concentrations of Sr in biotite decrease systematically from outer to inner aureole resulting in a progressive increase in measured $^{87}Rb/^{86}Sr$. Inset shows $^{87}Rb/^{86}Sr$ as a function of model age for each analysis (calculated assuming initial $^{87}Sr/^{86}Sr$ = 0.73). Dashed vertical lines mark timing of 1850 Ma regional metamorphism and 1322 Ma MLP crystallization. Error bars are 2σ

A simple volume-diffusion closure temperature scenario is not, however, universally applicable to biotite in the MLP aureole. For example, a sub-set of 17 analyses from armoured biotite inclusions in the outer aureole preserves an isochron age of 1850 ± 12 Ma that corresponds within error to zircon U-Pb ages obtained from migmatitic leucosomes in the regionally metamorphosed Tasiyuak Gniess. An important implication of this result is that it may be possible to recover prograde biotite Rb-Sr ages in upper-amphibolite to granulite(?) facies rocks if enough grains armoured in garnet, or another refractory mineral (e.g. quartz), are analysed. Lack of isotopic resetting in these fully armoured biotite grains reflects isolation from short-circuit pathways and slow diffusion of Sr in garnet: Giletti (1991) estimated an 8 order of magnitude slower Sr diffusion in garnet (log$D$ = -20) compared to biotite (log$D$ = -12) at 600 °C. Thus, a universal biotite Rb-Sr closure temperature is impossible to define based on this case study since the diffusion behaviour of Sr in biotite is dependent foremost on textural setting in addition to maximum temperature, cooling rate, mineral modes, and mineral chemistry. This observation illustrates the power of in situ Rb-Sr analyses to reveal hidden details of the *P-T-t* history that are beyond the reach of conventional mineral separation techniques

https://doi.org/10.5194/egusphere-2025-6320
Preprint. Discussion started: 31 December 2025

6.3 Biotite Rb-Sr behaviour in central aureole

Biotite in the central aureole occurs in a variety of textural settings depending on the extent of corona development. Biotite analyses were categorized as having sampled: 1) armoured grains; 2) partly liberated grains; 3) fully liberated grains. Partly and fully liberated grains display cuspate grain boundaries characteristic of net-transfer reactions. Tiny (<50 µm) biotite neoblasts are also part of the symplectitic assemblage in the central and inner aureole but are too small to analyse for in situ Rb-Sr.

Overall, the distribution of Rb-Sr data in central aureole samples is like that recorded in the outer aureole. This suggests similar intracrystalline and intergranular diffusion processes were at work at temperatures > 680 °C and cooling timescales of ~15 Myr. Armoured grains again record ~1850 Ma ages depending on localized connection of biotite inclusions with through going microfractures. The combination of Rb/Sr data, single-spot model ages, textures, and concentration data provide additional evidence for Sr diffusion as the main process accounting for resetting of Rb-Sr ages in the inner aureole. Whereas resorption of biotite might be expected to cause 'pile-up' zoning in Rb, there is little evidence for this process as recorded in the trace-element data. It seems likely, therefore, that growth of biotite neoblasts and rare K-feldspar acted as a sink for Rb liberated from resorbed regional metamorphic biotite. The youngest isochron calculated for fully liberated central aureole biotite is 1292.1 ± 6.5 Ma. This age is 23 My younger (taking upper error limit) than crystallization of the MLP at 1322 Ma and is similar to the timescales for heating and cooling below 500 °C in the central aureole produced by numerical and finite difference models. Thus, the youngest Rb-Sr isochron age in these samples provides evidence for biotite Rb-Sr T_c again in the neighbourhood of 500 °C.

6.4 Biotite Rb-Sr behaviour in inner aureole

Biotite neoblasts in the inner aureole are interpreted to have grown in textural equilibrium with the Opx + Crd symplectite assemblage. They display high Rb/Sr ratios resulting from very low Sr content and there is no evidence of a zone of partial retention as observed in the outer and central aureole. Despite the apparently homogeneous nature of the inner aureole dataset, the fact that half of the measurements have model ages >1322 Ma suggests there are other process at work beyond a simple diffusive closure mechanism. The *T-t* paths modelled for the inner aureole predict rapid heating to >800 °C followed by slow cooling below 500 °C after >25 Myr. Hence biotite neoblasts would be expected to record Rb-Sr ages <1300 Ma if Sr diffusion was efficient above 500 °C. The pooled isochron age is 1320.5 ± 7.0 Ma. The nuance in this inner aureole dataset is that individual neoblasts record strongly diffusion-controlled incorporation of Rb and Sr leading to grain-scale variations in $^{87}Rb/^{86}Sr$ such that the length scale of Rb and Sr diffusion during biotite neoblast growth was apparently shorter than the radius of a platy biotite grain (e.g. <200 µm). This is broadly consistent with work by Carlson (2010) who calculated seven orders of magnitude slower diffusion for Al in anhydrous versus fluid-saturated systems. This diffusion-controlled regime leads to two important processes that may not be recorded in the outer and central aureole: 1) each biotite

https://doi.org/10.5194/egusphere-2025-6320
Preprint. Discussion started: 31 December 2025

neoblast could have crystallized with a unique initial $^{87}Sr/^{86}Sr$ depending on the precursor mineralogy of the microdomain in which it nucleated; 2) slow intergranular diffusion could effectively armour biotite neoblasts from diffusive loss of Sr.

The possibility of a unique initial Sr for each neoblast arises from the fact that 1850 Ma regional metamorphic biotite inclusions with Rb/Sr between 50 and 100 would have ingrown Sr* to produce $^{87}Sr/^{86}Sr$ between 1.7 and 2.6 by 1322 Ma. Over the same ~530 Myr time interval, low Rb/Sr phases like garnet, apatite, and plagioclase would barely evolve above $^{87}Sr/^{86}Sr$ = 0.73. For example, Sousa et al. (2013) reports $^{87}Rb/^{86}Sr$ in garnet that averages ~0.10 with Sr concentrations between 0.1 and 100 ppm. Apatite in metamorphic settings typically contains 100-1000 ppm Sr (Tan et al., 2023; Bruand et al., 2017) and plagioclase analysed for initial $^{87}Sr/^{86}Sr$ in the MLP aureole contains 300 ± 40 ppm total Sr. Thus, biotite neoblasts that nucleated within a microdomain formerly occupied by a regional biotite inclusion might be expected to contain initial Sr significantly more radiogenic than the whole rock value. In contrast, biotite neoblasts nucleating away from these microdomains may have incorporated initial Sr closer to the whole rock. In this scenario the biotite neoblasts measured in a number of different coronas and across different samples might show a continuous range of initial $^{87}Sr/^{86}Sr$ between the whole rock value (0.73) and more radiogenic compositions. To test this scenario, it is possible to estimate the initial Sr value (I_{Sr}*) required to lower model ages to ≤1322 Ma. Doing so for inner aureole biotite neoblasts yields a continuous range of I_{Sr*} between 0.73 and 1.40. This type of behaviour is not expected in the outer and central aureoles where diffusive loss of Sr from biotite would not be expected to change the initial Sr value in relict regional biotite grains.

The evidence for short diffusive length scales for Rb and Sr during neoblast growth has implications for closure of Sr diffusion in the inner aureole. Biotite neoblasts are typically surrounded by vermicular low-Ca Opx + Crd neither of which has been studied for Sr volume diffusion at T > 800 °C (mostly owing to incompatible nature of large Sr^{2+} cation in these phases). However, Sr diffusion in diopside is better studied and extrapolates to logD < -23 at T < 900 °C (Sneeringer et al. 1984): this diffusivity is slower than experimental data for Sr diffusion in garnet. It is, therefore, possible that as biotite neoblasts finished crystallizing in the anhydrous low diffusivity coronal assemblages that it was also armoured from Rb-Sr resetting during subsequent cooling.

The raw regression age of 1320.5 ± 7.0 Ma for inner aureole neoblasts could easily be taken at face value. Unfortunately, the processes described above preclude this simple interpretation. It is more likely that individual biotite neoblasts record Rb-Sr ages ranging from ~1300 Ma to 1322 Ma depending on where they occur relative to precursor mineral domains and when, relative to the thermal pulse, the grains were isolated from intergranular Sr mobility.

6.5 Inner aureole biotite melt-pseudomorphs

Finally, biotite that forms as melt-pseudomorph films in sample T28-2m reveal contrasting behaviour compared to biotite neoblasts. As shown in Figure 3D above, these cuspate biotite films envelope sub-rounded quartz (and more rarely plagioclase) indicating that the latter was consumed during melt production. Despite analyzing biotite melt-pseudomorphs over a wide area of this thin section, the range of Rb/Sr is much narrower than biotite neoblasts: Rb/Sr = 508-825 with a

https://doi.org/10.5194/egusphere-2025-6320
Preprint. Discussion started: 31 December 2025

mean of 637 ± 83 (1σ; 13%) for melt films compared to 38-2800 with mean of 1270 ± 675 (1σ; 53%) for biotite neoblasts in sample M02C-10m. The most obvious process that could account for the more homogeneous Rb-Sr in biotite melt films is the longer-range three-dimensional connectivity of melt pockets, faster diffusion of Rb and Sr through silicate melts, and the mobile nature of high-T silicate melt allowing for advective mixing. These features would promote elemental and isotopic homogenization at the scale of cm rather than µm and over timescales of a few Myr at T > 800 °C in the inner aureole. The narrow range of Rb/Sr places more importance on the correct choice for initial $^{87}Sr/^{86}Sr$. At this distance in the aureole, the biotite must have crystallized at ≤1322 Ma and this necessarily restricts the initial $^{87}Sr/^{86}Sr$ to ≥ 0.85. Efficient intercrystalline Sr diffusion at T > 800 °C would also promote open-system behaviour and closure ages <1300 Ma. There is some evidence for long-lived open-system behaviour as recorded by the four youngest spots that produce an anchored (at initial Sr = 0.85) isochron age of 1293 ± 14 Ma. More work will be needed to check the veracity of the proposed higher initial value and for open system behaviour. The initial Sr of the low-degree partial melts recorded by these biotite melt pseudomorphs could, for instance, reflect the balance and abundance of K-feldspar + biotite relative to plagioclase + quartz in the melting reaction: melting higher proportions of K-feldspar + biotite would produce more radiogenic initial $^{87}Sr/^{86}Sr$. This process is envisioned to represent the incipient stage in the eventual accumulation of anatectic melt into larger isotopically homogeneous granitic plutons. Higher-than-expected initial $^{87}Sr/^{86}Sr$ in partial melts has also been observed in Himalayan leucogranites (Yang et al., 2022) where preferential melting of muscovite has been attributed to elevated initial Sr values.

7 Conclusions

In contrast to previous studies of Rb-Sr closure in biotite, the use of in situ LA MS/MS-ICP-MS provides unprecedented insight into the grain-scale controls on diffusion behaviour in cooling rocks. In the current study, the use of in situ Rb-Sr measurements reveals that the exact microtextural setting of biotite ultimately controlled the behaviour of the Rb-Sr system. Pervasive Rb-Sr resetting occurred only when biotite inclusions were connected to the surrounding matrix by microfractures that provided short-circuit pathways for diffusion through garnet. Open-system behaviour of Sr in biotite above 500 °C in the outer aureole is at the upper limit of Rb-Sr biotite T_c proposed by von Blankenburg et al. (1989); it is impossible to place a lower limit on Sr diffusion in the MLP aureole but it is noteworthy that only 2 of 88 analyses in the outer aureole returned a model age <1322 Ma yet thermal models predict >15 Myr to cool below 500 °C. This hints at T_c for Sr diffusion closer to the upper range of existing estimates. A subset of biotite spots in the central aureole with an isochron age of 1291.1 ± 6.5 Ma is also consistent with closure of Rb-Sr in biotite after prolonged cooling to T < 500 °C.

Another key benefit of examining closure systematics in high-T contact aureoles is that confidence can be attributed to isochron ages that are significantly younger than magmatic crystallization age. Here the thermal models predict T-t paths for heating and cooling below 500 °C that span 5 to >20 Myr depending on distance from the intrusive contact. Small subsets of data that record isochron ages <1300 Ma can be confidently attributed to open-system behaviour and canonical closure during cooling below T_c. This study also emphasizes that large datasets (e.g. >100 spots) may sometimes be required

https://doi.org/10.5194/egusphere-2025-6320
Preprint. Discussion started: 31 December 2025

to reveals zones of partial retention and tails on 'S'-shaped linearized probability plots that could be used to calculate meaningful cooling ages. More in situ Rb-Sr dating studies in similarly well-constrained, lower-temperature, natural settings are required to expand the lower limit of Sr diffusion in biotite.

In some cases, however, 1850 Ma biotite Rb-Sr ages are preserved as long as the grains remained isolated from short-circuit diffusion. This implies that the use of biotite Rb-Sr should not be disregarded in upper-amphibolite and granulitic rocks: the challenge is to find biotite in textural settings (e.g. armoured grains) that may preserve prograde ages. Biotite armoured in quartz in granulitic rocks might be expected to display similar behaviour. Work by Tattelaar & Indares (2007) estimated regional metamorphic *P-T* conditions for the Tasiyuak Gneiss in the same vicinity as the present study of ~870 °C at 8-10 kbar and regional metamorphic biotite contains 4.5 to 5.7 wt% TiO_2 and 1.91 to 1.97 wt% F with only minor Cl. It is possible, therefore, that other granulitic and UHT rocks may contain biotite that records prograde Rb-Sr ages. Rounded biotite inclusions in peritectic minerals such as cordierite, sapphirine, orthopyroxene, and garnet (e.g. Bose et al., 2005; Guo et al., 2024) attest to dehydration of biotite sometimes at conditions in excess of 900°C at 8 kbar. Refined thermodynamic solution models for high-*T* breakdown of Ti- and Fe^{3+} biotite (e.g. Tajčmanová et al., 2009) also allow *P-T* pseudosection calculations in the NCKFMASHTO system; this ties armoured biotite Rb-Sr ages directly to prograde reactions in the major mineral assemblage: no such capacity currently exists for U-Pb ages from accessory minerals like zircon or monazite. Thus, demonstrating prograde Rb-Sr ages preserved in UHT biotite armoured in peritectic phases would be a valuable addition to geochronology in high-grade rocks and future work will attempt to test this hypothesis. The response of biotite armoured in other high Rb/Sr phases like K-felspar, or low Rb/Sr phases like plagioclase could also be explored using in situ methods; these inclusion/host isotopic measurements might ultimately yield robust cooling ages if zoning profiles for Rb, Sr, Rb/Sr and $^{87}Sr/^{86}Sr$ are combined with volume diffusion data for Sr and Rb (e.g. Giletti, 1991) in these mineral pairs. Exploring such biotite (or muscovite) inclusion/host relationships using in situ methods is another fruitful avenue for further research.

References

Armstrong, R. L., Jäger, E., and Eberhardt, P.: A comparison of K-Ar and Rb-Sr ages on Alpine biotites, Earth and Planetary Science Letters, 1, 13–19, 1966.

Bertrand, J.-M., Van Kranendonk, M., Hanmer, S., Roddick, J. C., and Ermanovics, I.: Structural and metamorphic geochronology of the Torngat Orogen in the North River-Nutak transect area, Labrador: Preliminary results of U-Pb dating, Geoscience Canada, 1990.

Bose, S., Das, K., and Fukuoka, M.: Fluorine content of biotite in granulite-grade metapelitic assemblages and its implications for the Eastern Ghats granulites, European Journal of Mineralogy, 17, 665–674, 2005.

Bruand, E., Fowler, M., Storey, C., and Darling, J.: Apatite trace element and isotope applications to petrogenesis and provenance, American Mineralogist, 102, 75–84, 2017.

https://doi.org/10.5194/egusphere-2025-6320
Preprint. Discussion started: 31 December 2025

Carlson, W.: Dependence of reaction kinetics on H2O activity as inferred from rates of intergranular diffusion of aluminium, Journal of Metamorphic Geology, 28, 735–752, 2010.

Chiaradia, M., Schaltegger, U., Spikings, R., Wotzlaw, J.-F., and Ovtcharova, M.: How accurately can we date the duration of magmatic-hydrothermal events in porphyry systems?—an invited paper, Economic Geology, 108, 565–584, 2013.

Dodson, M.: Theory of cooling ages, in: Lectures in isotope geology, Springer, 194–202, 1979.

Dodson, M. H.: Closure temperature in cooling geochronological and petrological systems, Contributions to Mineralogy and Petrology, 40, 259–274, 1973.

Ehlers, K. and Powell, R.: An empirical modification of Dodson's equation for closure temperature in binary systems, Geochimica et cosmochimica Acta, 58, 241–248, 1994.

Ganguly, J. and Tirone, M.: Diffusion closure temperature and age of a mineral with arbitrary extent of diffusion: theoretical formulation and applications, Earth and Planetary Science Letters, 170, 131–140, 1999.

Giletti, B.: Rb and Sr diffusion in alkali feldspars, with implications for cooling histories of rocks, Geochimica et Cosmochimica Acta, 55, 1331–1343, 1991.

Glodny, J., Kühn, A., and Austrheim, H.: Diffusion versus recrystallization processes in Rb–Sr geochronology: isotopic relics in eclogite facies rocks, Western Gneiss Region, Norway, Geochimica et Cosmochimica Acta, 72, 506–525, 2008.

Guo, M., Zhang, J., Qian, J., Yin, C., Gao, P., Hsia, J., Zhang, S., and Yu, C.: Ultrahigh-temperature metamorphism of the felsic granulites in the eastern North China Craton and their implications on the Neoarchean tectonic regime, Lithos, 468, 107516, 2024.

Hanson, G. and Gast, P.: Kinetic studies in contact metamorphic zones, Geochimica et Cosmochimica Acta, 31, 1119–1153, 1967.

Harrison, T. M. and Clarke, G. K.: A model of the thermal effects of igneous intrusion and uplift as applied to Quottoon pluton, British Columbia, Canadian Journal of Earth Sciences, 16, 411–420, 1979.

Hogmalm, K. J., Zack, T., Karlsson, A. K.-O., Sjöqvist, A. S., and Garbe-Schönberg, D.: In situ Rb–Sr and K–Ca dating by LA-ICP-MS/MS: an evaluation of N 2 O and SF 6 as reaction gases, Journal of Analytical Atomic Spectrometry, 32, 305–313, 2017.

Holness, M. B. and Clemens, J. D.: Partial melting of the Appin Quartzite driven by fracture-controlled H2O infiltration in the aureole of the Ballachulish Igneous Complex, Scottish Highlands, Contributions to Mineralogy and Petrology, 136, 154–168, 1999.

Jenkin, G. R., Ellam, R. M., Rogers, G., and Stuart, F. M.: An investigation of closure temperature of the biotite Rb-Sr system: The importance of cation exchange, Geochimica et Cosmochimica Acta, 65, 1141–1160, 2001.

Jenkin, G. R. T., Rogers, G., Fallick, A. E., and Farrow, C. M.: Rb-Sr closure temperatures in bi-mineralic rocks: a mode effect and test for different diffusion models, Chemical Geology, 122, 227–240, https://doi.org/10.1016/0009-2541(95)00013-C, 1995.

https://doi.org/10.5194/egusphere-2025-6320
Preprint. Discussion started: 31 December 2025

Kelly, E., Carlson, W., and Connelly, J.: Implications of garnet resorption for the Lu–Hf garnet geochronometer: an example from the contact aureole of the Makhavinekh Lake Pluton, Labrador, Journal of Metamorphic Geology, 29, 901–916, 2011.

Larson, K. P., Shrestha, S., Button, M., Cottle, J. M., and Barnes, C. J.: The Effect of Crystal Orientation on In Situ Rb-Sr Mica Geochronology, Geostandards and Geoanalytical Research, 49, 705–713, 2025.

Lightfoot, P. C., Keays, R. R., Evans-Lamswood, D., and Wheeler, R.: S saturation history of Nain Plutonic Suite mafic intrusions: origin of the Voisey's Bay Ni–Cu–Co sulfide deposit, Labrador, Canada, Mineralium Deposita, 47, 23–50, 2012.

Ludwig, K. R.: User's manual for Isoplot 3.75: A geochronological toolkit for Microsoft Excel, Berkeley Geochronology Center Special Publication, 5, 75, 2012.

Mariga, J., Ripley, E., and Li, C.: Petrologic evolution of gneissic xenoliths in the Voisey's Bay Intrusion, Labrador, Canada: Mineralogy, reactions, partial melting, and mechanisms of mass transfer, Geochemistry, Geophysics, Geosystems, 7, 2006.

McFarlane, C., Carlson, W., and Connelly, J.: Prograde, peak, and retrograde P–T paths from aluminium in orthopyroxene: High-temperature contact metamorphism in the aureole of the Makhavinekh Lake Pluton, Nain Plutonic Suite, Labrador, Journal of Metamorphic Geology, 21, 405–423, 2003a.

McFarlane, C. R. and Harrison, T. M.: Pb-diffusion in monazite: constraints from a high-T contact aureole setting, Earth and Planetary Science Letters, 250, 376–384, 2006.

McFarlane, C. R., Connelly, J. N., and Carlson, W. D.: Monazite and xenotime petrogenesis in the contact aureole of the Makhavinekh Lake Pluton, northern Labrador, Contributions to Mineralogy and Petrology, 148, 524–541, 2005a.

McFarlane, C. R., Connelly, J. N., and Carlson, W. D.: Intracrystalline redistribution of Pb in zircon during high-temperature contact metamorphism, Chemical Geology, 217, 1–28, 2005b.

McFarlane, C. R. M., Carlson, W. D., and Connelly, J. N.: Prograde, peak, and retrograde P-T paths from aluminium in orthopyroxene: High-temperature contact metamorphism in the aureole of the Makhavinekh Lake Pluton, Nain Plutonic Suite, Labrador, Journal of Metamorphic Geology, 21, 405–423, 2003b.

Mengel, F. and Rivers, T.: Metamorphism in the Paleoproterozoic Torngat Orogen, Labrador: Petrology and P-T-t paths of amphibolite- and granulite-facies rocks across the Komaktorvik shear zone, Canadian Mineralogist, 35, 1137–1160, 1997.

Mengel, F., Rivers, T., and Reynolds, P.: Lithotectonic elements and tectonic evolution of Torngat Orogen, Saglek Fiord, northern Labrador, Canadian Journal of Earth Sciences, 28, 1407–1423, 1991.

Müller, W., Mancktelow, N. S., and Meier, M.: Rb–Sr microchrons of synkinematic mica in mylonites: an example from the DAV fault of the Eastern Alps, Earth and Planetary Science Letters, 180, 385–397, 2000.

Nebel, O.: Rb-Sr dating, in: Encyclopedia of scientific dating methods, Springer, 686–698, 2015.

Percival, J. and Peterman, Z.: Rb–Sr biotite and whole-rock data from the Kapuskasing uplift and their bearing on the cooling and exhumation history, Canadian Journal of Earth Sciences, 31, 1172–1181, 1994.

Ribeiro, B. V., Kirkland, C. L., Finch, M. A., Faleiros, F. M., Reddy, S. M., Rickard, W. D., and Hartnady, M. I.: Microstructures, geochemistry, and geochronology of mica fish: Review and advances, Journal of structural geology, 175, 104947, 2023.

https://doi.org/10.5194/egusphere-2025-6320
Preprint. Discussion started: 31 December 2025

Rivers, T., Mengel, F., Scott, D. J., Campbell, L. M., and Goulet, N.: Torngat Orogen—a Palaeoproterozoic example of a narrow doubly vergent collisional orogen, Geological Society, London, Special Publications, 112, 117–136, 1996.

Ryan, B.: Makhavinekh lake pluton, Labrador, Canada: geological setting, subdivisions, mode of emplacement, and a comparison with Finnish rapakivi granites, Precambrian Research, 51, 193–225, 1991.

Scott, D. J. and Machado, N.: UPb geochronology of the northern Torngat Orogen, Labrador, Canada: a record of Palaeoproterozoic magmatism and deformation, Precambrian Research, 70, 169–190, 1995.

Sneeringer, M., Hart, S. R., and Shimizu, N.: Strontium and samarium diffusion in diopside, Geochimica et Cosmochimica Acta, 48, 1589–1608, 1984.

Sousa, J., Kohn, M. J., Schmitz, M. D., Northrup, C. J., and Spear, F.: Strontium isotope zoning in garnet: implications for metamorphic matrix equilibration, geochronology and phase equilibrium modelling, Journal of Metamorphic Geology, 31, 437–452, 2013.

Tajčmanová, L., Connolly, J., and Cesare, B.: A thermodynamic model for titanium and ferric iron solution in biotite, Journal of Metamorphic Geology, 27, 153–165, 2009.

Tan, H. M. R., Huang, X.-W., Meng, Y.-M., Xie, H., and Qi, L.: Multivariate statistical analysis of trace elements in apatite: Discrimination of apatite with different origins, Ore Geology Reviews, 153, 105269, 2023.

Tettelaar, T. and Indares, A.: Granulite-facies regional and contact metamorphism of the Tasiuyak paragneiss, northern Labrador: textural evolution and interpretation, Canadian Journal of Earth Sciences, 44, 1413–1437, 2007.

Thirlwall, M. and Burnard, P.: Pb-Sr-Nd isotope and chemical study of the origin of undersaturated and oversaturated shoshonitic magmas from the Borralan pluton, Assynt, NW Scotland, Journal of the Geological Society, 147, 259–269, 1990.

v. Blanckenburg, F., Villa, I., Baur, H., Morteani, G., and Steiger, R.: Time calibration of a PT-path from the Western Tauern Window, Eastern Alps: the problem of closure temperatures, Contributions to mineralogy and Petrology, 101, 1–11, 1989.

Van Kranendonk, M. J.: Tectonic evolution of the Paleoproterozoic Torngat Orogen: Evidence from pressure-temperature-time-deformation paths in the North River map area, Labrador, Tectonics, 15, 843–869, 1996.

Whitney, D. L. and Evans, B. W.: Abbreviations for names of rock-forming minerals, American Mineralogist, 95, 185–187, 2010.

Willigers, B., Mezger, K., and Baker, J.: Development of high precision Rb–Sr phlogopite and biotite geochronology; an alternative to 40Ar/39Ar tri-octahedral mica dating, Chemical Geology, 213, 339–358, 2004.

Wohletz, K., Civetta, L., and Orsi, G.: Thermal evolution of the Phlegraean magmatic system, Journal of Volcanology and Geothermal Research, 91, 381–414, 1999.

Yang, L., Wang, J.-M., Liu, X.-C., Khanal, G. P., and Wu, F.-Y.: Sr-Nd-Hf Isotopic Disequilibrium during the partial melting of metasediments: insight from Himalayan leucosome, Frontiers in Earth Science, 10, 891960, 2022.

https://doi.org/10.5194/egusphere-2025-6320
Preprint. Discussion started: 31 December 2025

Zack, T. and Hogmalm, K. J.: Laser ablation Rb/Sr dating by online chemical separation of Rb and Sr in an oxygen-filled reaction cell, Chemical Geology, 437, 120–133, 2016. B. B. and Carter, C.: The test article, J. Sci. Res., 12, 135–147, doi:10.1234/56789, 2015.

Smith, A. A., Carter, C., and Miller, B. B.: More test articles, J. Adv. Res., 35, 13–28, doi:10.2345/67890, 2014.